Sensors and Materials, Vol. 36, No. 7 (2024) 3147–3165
MYU Tokyo

S & M 3723

Variability of Land Surface Temperatures in Beijing's Historic Districts

Meizi Yang*

School of Architecture and Urban Planning, Beijing University of Civil Engineering and Architecture, Beijing 100044, China

(Received June 18, 2024; accepted July 26, 2024)

Keywords: land surface temperatures, historic districts, environmental evaluation, mitigation strategy, urban morphology

In recent years, the conflict between human activities and the natural environment has led to global warming and the emergence of extreme weather events, prompting reflection on the climate adaptability of buildings. Historical and cultural districts often reflect the design and construction strategies of their era, which were shaped by the prevailing social environments and natural conditions, so they typically embody construction techniques tailored to address local climatic characteristics. Consequently, in this paper, we focus on 33 historic and cultural districts within Beijing's old city, along with seven proposed historic and cultural districts, to retrieve land surface temperatures (LST) using Landsat remote sensing data and radiative transfer equations. A spatiotemporal analysis was conducted to investigate the variations in LST distribution across different historic and cultural districts and to characterize the internal temperature features within the historic and cultural districts of Beijing's old city. Research indicates the following: (1) The Dashilan area boasts the highest average LST, while the Huangcheng area records the lowest. (2) Over the past six years, most historic and cultural districts have experienced a decline in LST. Notably, the most significant reductions in average LST have been observed in the areas west of Xinjiekou, Dongsi South, and from the 3rd to the 8th Street in Dongsi. (3) Within the historic and cultural districts, hot spots of LST are primarily concentrated in the residential areas with one-story traditional houses, while cold spots are predominantly found around water, cultural relics, and modern architectural structures.

1. Introduction

Beijing, as an ancient city with a history spanning millennia, boasts a foundation of 3000 years and a history as a capital of 1000 years. The city's long history has endowed it with an inestimable wealth of historical relics, contributing to a distinct urban cityscape. Historical and cultural districts, owing to their preservation of a plethora of cultural relics and ancient sites, their concentrated distribution of traditional architectures, and their continuation in traditional

*Corresponding author: e-mail: 1108130321002@stu.bucea.edu.cn
https://doi.org/10.18494/SAM5188

ISSN 0914-4935

public spaces, represent the quintessential loci where the essence of Beijing's historical ambiance is most vividly manifested.[1]

The design and construction methods for traditional architecture often embody profound considerations tailored to regional climate adaptability.[2,3] During the initial stages of construction, designers employ the most economical methods to create an optimal architectural environment, considering factors such as site selection, floor plan layout, spatial creation, building materials, and construction techniques.[3–6] From the perspective of modern physics, this involves understanding the local climate and applying principles such as the chimney effect, heat absorption through phase change evaporation, soil heat absorption, and solar energy utilization. These principles are used to rationally arrange the building's floor plan, effectively organize its spaces, and optimize its form, integrating it with the surrounding environment to create comfortable indoor and outdoor environments.[5,6] The traditional Beijing Siheyuan (a traditional courtyard-style residence in Beijing), as a representative of Beijing's architecture, stands out for its remarkable climate adaptability. Its design and construction techniques offer valuable insights for the study and improvement of urban thermal environments.

In response to socioeconomic transformation, current plans for updating historic districts often redevelop existing residential buildings for commercial purposes, increasing the use of high-energy-consuming equipment and consequently anthropogenic heat emissions.[7–9] To meet the demands of urban living, pervious surfaces within historic districts are often replaced with impervious hardscapes, significantly increasing the proportion of impervious surfaces. Architectural additions are often built upon existing courtyard layouts to accommodate more people, resulting in the erosion of public spaces and green areas, making them smaller and more fragmented horizontally. Vertically, these additions increase building heights and compromise the original sloping roof architecture. Therefore, studying the thermal environment of historic districts reveals unique thermal issues present in these areas today.[8,10] On the basis of this, appropriate improvement strategies can be proposed to enhance the thermal comfort of these districts.

In studying the thermal environment of historical districts, it is essential to consider the surface temperature. The methods for retrieving land surface temperature primarily include the monowindow algorithm, the split-window algorithm, and the radiative transfer equation, differing principally in their underlying principles and computational complexity. Specific advantages, disadvantages, and scopes of application are as follows:

(1) Monowindow algorithm: The monowindow algorithm is an inversion technique rooted in statistical principles. It involves selecting a fixed-size window to compute the average radiant temperature and atmospheric temperature of the pixels within it, and then using the radiative transfer equation to deduce the surface temperature. This method is computationally straightforward and highly real-time, making it suitable for extensive real-time monitoring.[11–13] However, it is sensitive to the choice of window size; an inappropriate selection may compromise accuracy.

(2) Split-window algorithm: The split-window algorithm is an inversion technique rooted in recursive partitioning, which subdivides a large window into numerous smaller ones and determines the window size from the data distribution within.[14–16] In contrast to the

monowindow algorithm, the split-window algorithm offers adaptive window resizing, enhancing precision and stability, making it well-suited for extensive real-time monitoring. However, its computational demands preclude its suitability for real-time processing.

(3) Radiative transfer equation: The radiative transfer equation represents an inversion technique rooted in physical models, which computes surface temperature by accounting for physical processes such as surface reflection and atmospheric radiative transfer. This method is distinguished by its high precision and robust reliability, making it well-suited for high-accuracy retrievals and scientific research. However, it necessitates an extensive array of physical parameters and computational time, rendering it computationally intensive and not ideally suited for real-time processing.[16,17]

The monowindow and split-window algorithms are well-suited for extensive real-time monitoring, whereas the radiative transfer equation is more appropriate for high-resolution land surface temperature retrieval. Consequently, in this study, we employed the radiative transfer equation to invert urban land surface temperatures on the basis of The Thermal Infrared Sensor (TIRS) bands from Landsat 8 and Landsat 9.[15]

However, existing studies on the renovation and transformation of historic districts tend to focus more on aspects such as cultural history, preservation of historical architecture,[8] commercial development,[18] and enhancement of vibrancy,[19] with lesser consideration given to the climatic factors that influence architectural layout and spatial organization.[20] In the limited specialized research on the adaptability of buildings to climate in the Beijing region, most studies are directed at individual historic courtyards or buildings, lacking a comparative analysis across different historic districts. In terms of temporal dimensions, research predominantly employs empirical measurements or simulations to assess microclimate on a single day, with a dearth of studies focusing on long-term sequences. In depth, research is confined to discussions on principles and norms, design strategies, or the direct application of established foreign green building techniques, devoid of site-specific studies. Consequently, in this paper, we take 33 historic and seven proposed cultural districts in the old city of Beijing as case studies, utilizing satellite remote sensing data to conduct multi-year land surface temperature inversions. We employ methods such as hotspot analysis and linear regression to investigate the characteristics of land surface temperature distribution within the various historic districts and the interaction between the built environment and land surface temperature, aiming to ameliorate the thermal environment and enhance the livability of these historic districts.

2. Study Area and Method

2.1 Study area

In this study, we focus on the historical and cultural districts within the old city of Beijing, as well as the proposed new historical districts. The Beijing municipal government has issued three batches of announcements designating a total of 33 historical and cultural districts, encompassing an area of 2063 hectares, which represents 33% of the old city's total area. Within this area, there are 15 historical districts located inside the imperial city, covering approximately 680 hectares,

and 18 districts outside the imperial city, amounting to 1383 hectares. These include areas such as Dashilan (DSL), Guozijian-Yonghegong (GZJ-YHG), Nanluoguxiang (NLGX), Beiluguxiang (BLBX), Shichahai (SCH), 3rd to the 8th Street in Dongsi t (DSST-BT), Zhangzizhong Road South (ZZZLN), Zhangzizhong Road North (ZZZLB), Xintaicang (XTC), Dongsi South (DSN), Fuchengmen Inner Street (FCMNDJ), 1st to the 8th Street in Xisi North (XSB-BT), Naoshikou South (NNSK), Dongjiaominxiang (DJMX), Fayuan Temple (FYS), West Liulichang (XLIC), East Liulichang (DLIC), and Xianyukou (XYK). Additionally, the study includes seven proposed historical and cultural districts in the regulatory detailed planning of the capital's functional core area, which are Xinjiekou West (XJK), Huangcheng West (HCX), Huangcheng East (HCD), Zhuanta Hutong (ZTHT), Shibei Hutong (SBHT), Zhanxi Street (ZXJ), and Xiangchang New Urban Area (XCXSQ) (Fig. 1).

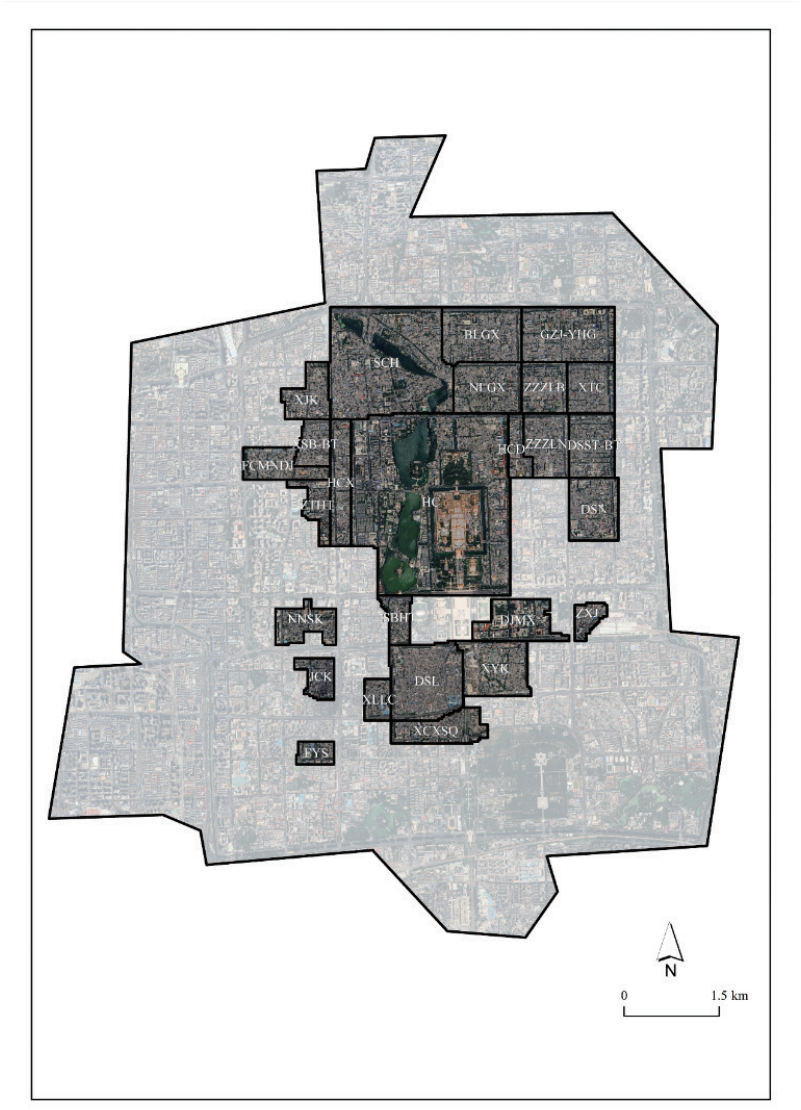

Fig. 1. (Color online) Study area.

In terms of the thermal environment, we conducted an on-site inspection of the old city and compiled data on the floor area ratio (*FAR*), building density (*BD*), mean building height (*MBH*), and fraction of vegetation coverage (*FVC*) (Table 1), and we found that within the historic and cultural districts of Beijing's old city, the dense population and architecture, coupled with high levels of construction activity, have generated considerable thermal sources. Additionally, the monolithic pavement in these historic areas, with limited use of permeable materials, is not conducive to maintaining a balanced humid environment, resulting in lower humidity levels. Furthermore, the generally narrower streets in the historic districts have suboptimal air circulation, impeding the rapid dispersion of temperature. These factors collectively contribute to elevated air and surface temperatures within the cultural and historic districts, manifesting a pronounced heat island effect.

2.2 Methods

2.2.1 Radiative transfer equation

The fundamental principle of the radiative transfer equation is to delineate the interplay between thermal radiation within the atmosphere and Earth's surface. This principle enables the

Table 1
Summary of urban block morphological data.

Layer	*FAR*	*BD*	*MBH*	*FVC*
BLGX	0.769	0.425	24.000	0.216
DJMX	1.291	0.306	57.000	0.253
DSL	0.775	0.373	36.000	0.085
DSN	1.254	0.408	69.000	0.161
DSST-BT	0.808	0.465	33.000	0.176
FCMNDJ	0.717	0.460	36.000	0.130
FYS	0.756	0.346	21.000	0.242
GZJ-YHG	0.885	0.405	45.000	0.178
HC	0.568	0.257	57.000	0.225
HCD	1.001	0.344	60.000	0.228
HCX	1.068	0.420	48.000	0.154
JCK	0.767	0.473	57.000	0.174
NLGX	0.630	0.439	27.000	0.203
NNSK	0.907	0.340	42.000	0.177
SBHT	0.507	0.352	33.000	0.193
SCH	0.678	0.367	72.000	0.215
XCXSQ	0.822	0.365	48.000	0.112
XJK	0.870	0.430	51.000	0.135
XLIC	0.609	0.391	36.000	0.151
XSB-BT	0.786	0.556	39.000	0.132
XTC	0.693	0.516	33.000	0.183
XYK	0.642	0.312	39.000	0.209
ZTHT	1.178	0.444	36.000	0.217
ZXJ	1.055	0.334	42.000	0.141
ZZZLB	1.038	0.390	57.000	0.212
ZZZLN	0.993	0.416	33.000	0.135

representation of the thermal infrared radiance received by a satellite as the sum of three components: atmospheric upward radiance $L\uparrow$, the true terrestrial radiance traversing the atmosphere, and the downward reflected energy from the atmosphere. Consequently, the radiative transfer equation serves to compute the thermal infrared radiance L_λ received by the satellite, expressed as[17]

$$L_\lambda = \left[\varepsilon B\left(T_S\right) + \left(1-\varepsilon\right)L\downarrow\right]\tau + L\uparrow . \tag{1}$$

In the equation, ε represents the surface emissivity, T_S denotes the true surface temperature (in Kelvin), $B(TS)$ signifies the brightness of a blackbody at temperature T_S, and τ stands for the atmospheric transmittance in the thermal infrared range. $L\uparrow$ and $L\downarrow$ are atmospheric profile parameters respectively representing the upward and downward radiance of the atmosphere. These atmospheric profile parameters can be calculated and obtained from the website http://atmcorr.gsfc.nasa.gov/.

The radiance $B(TS)$ of a blackbody at temperature T in the thermal infrared spectrum is given by

$$B\left(T_S\right) = \left[L_\lambda - L\uparrow - \tau(1-\varepsilon)L\downarrow\right] / \tau\varepsilon . \tag{2}$$

According to Planck's formula, T_S can be expressed as

$$T_S = \frac{K2}{\ln\left[\dfrac{K1}{B\left(T_S\right)}\right]} + 1 . \tag{3}$$

In the equation, $K1$ and $K2$ represent preset constants prior to satellite launch. For TIRS Band 10, $K1$ is set at 774.89 W/(m^2 × μm × sr) and $K2$ at 1321.08 K.

Through the methodologies, the LST of Beijing's core area from 2017 to 2023 was inversely derived.

2.2.2 Methods for spatial distribution characteristics

The Getis-Ord Gi* statistical tool identifies hot/cold spots with statistical significance by correlating the LST of each grid with its statistical neighbors. Therefore, an isolated high LST value does not constitute a hot spot, nor does an isolated low LST value constitute a cold spot. A spot is considered hot/cold only if the LST within a single grid and its adjacent grids are both high/low. Compared with heat maps, hot spot analysis can reveal hidden information and present it in different confidence spaces, resulting in a more objective visualization. The specific calculation formula is[21]

$$G^* = \frac{\sum_{j=1}^{n} W_{ij} X_j}{\sum_{j=1}^{n} X_J}. \tag{4}$$

In the formula, G^* represents the Getis-Ord* statistic; X_j denotes the attribute value of the j-th spatial unit; n signifies the LST within the grid; and W_{ij} stands for the spatial weight matrix. A positive G^* indicates high-value clustering, referred to as hot spots, while a negative G^* indicates low-value spatial clustering, known as cold spots.

3. Results

3.1 Climatic context-spatiotemporal characteristics of LST in the core area of Beijing

Historic districts are neither hermetic nor exist independently from external influences; rather, they are subject to mutual impacts with their climatic environments and surrounding regions. Consequently, prior to studying historic districts, we first examined the spatiotemporal distribution of surface temperatures in the core area of Beijing. To visually represent this distribution, we conducted surface temperature inversions and spatial information visualizations for the core area during the summer periods of 2017, 2020, and 2023.

Analysis of the LST inversion results from 2017 to 2023 depicted in Fig. 2 reveals that the summer LST in the core area of Beijing ranges from 37 to 63 °C, exhibiting a spatial distribution characterized by a "low-high-low" annular pattern. The central HC region is dominated by low values, with relatively concentrated low-temperature areas also present at the periphery of the core zone, such as around the Temple of Heaven Park. Conversely, the majority of high-temperature regions are concentrated in the historical districts outside the HC, including areas such as DSL, XJK, and FCMNDJ.

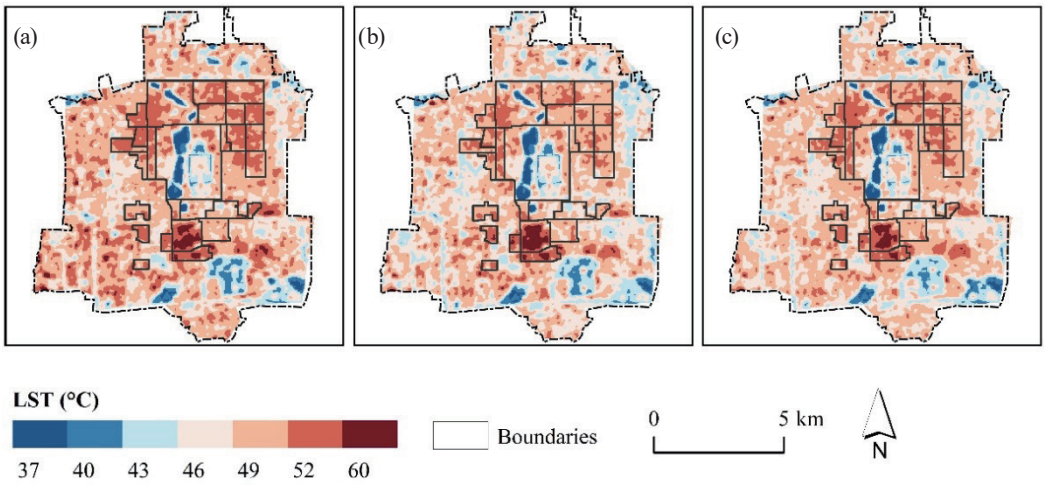

Fig. 2. (Color online) Spatial distribution of LST in the core area of Beijing: (a) 2017, (b) 2020 and (c) 2023.

In the temporal dimension, the LST within the core area exhibited an initial decline followed by an increase from 2017 to 2023. Between 2017 and 2020, a notable reduction in surface temperatures was observed across the core area, except for DSL, particularly evident in the Siheyuan residential areas. From 2020 to 2023, a slight uptick in surface temperatures was noted within the core area; however, these temperatures still represented a decrease when compared with 2017 levels.

On the basis of the above research on the spatial and temporal distribution characteristics of LST in the core area of Beijing, we can find that from the spatial dimension, the thermal environment problems in historical and cultural districts (except for HC) are more serious than those in other areas in the core area and should be focused on. From the temporal dimension, with the population evacuation and environmental remediation of residential bungalow, the thermal environment problems in historical districts have been improved to some extent.

3.2 Horizontal comparison - differences in average surface temperature between different historical and cultural blocks

Having initially clarified the spatiotemporal distribution of LST within the core districts of Beijing, our research narrows down to various historical cultural districts to explore the disparities in LST among them, as well as the characteristics of LST's spatiotemporal distribution within each historic district.

Figure 3 illustrates the average LST of various historical districts over the years 2017, 2020, and 2023. The findings indicate that the average LST in DSL and the adjacent XCXSQ surpasses that of other historic and cultural districts, while the average LST in the HC is notably lower than those in the other districts. Furthermore, Fig. 3 reveals a discernible decline in the average LST of XJK, DSN, and DSST-BT over the six-year period.

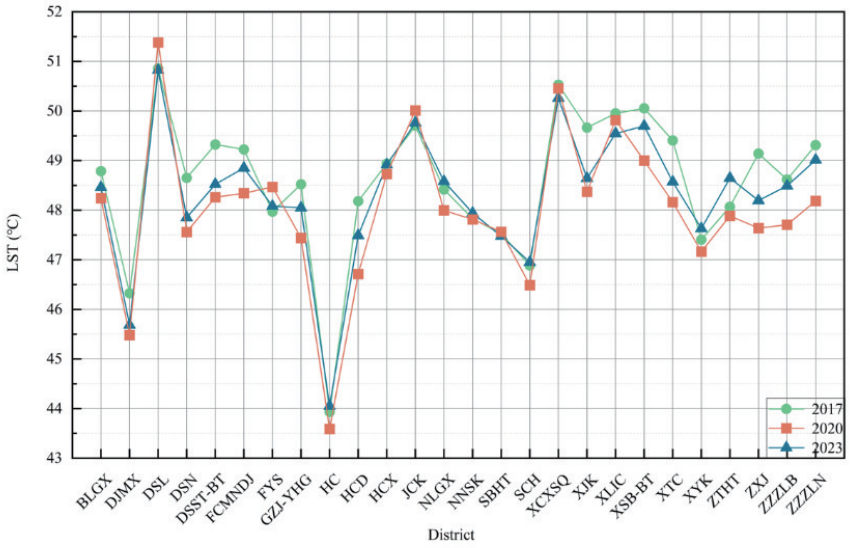

Fig. 3. (Color online) Mean LST observed in historical districts in the years 2017, 2020, and 2023.

The reasons for the differences in surface temperature among different historical districts are related to their urban morphology, functions, and socioeconomic factors. Taking DSL as an example, it has a high building density in terms of urban morphology and lacks public spaces for greening. Functionally, DSL is one of the most famous commercial streets in the core area of Beijing, where commercial buildings consume more energy than residential buildings. At the same time, with the influx of a large number of tourists, the emission of anthropogenic heat in this area will increase significantly, exacerbating the problem of thermal environment. In contrast, HC is mainly used for cultural tourism and government offices. To attract tourists and create a solemn government office environment, the urban texture of this area is well preserved, with low building density and good greening landscape. In addition, there are rivers flowing through the area, so the surface temperature is relatively lower in this area than in other historical districts.

Figure 4 further presents the boxplot analysis of LST across various historical districts in 2017, 2020, and 2023. The upper and lower extremes of the boxplot reveal that DSL has the highest upper extreme value, indicating the plots with the highest LST, reaching 54.72 °C. In contrast, SBHT has the lowest upper extreme value, with the highest LST plot reaching only 49.62 °C, nearly 5 °C lower than that in DSL. HC exhibits the lowest lower extreme value, with the lowest LST plot at 32.56 °C, significantly lower than in other historical districts. XSB-BT has the highest lower extreme value, with the lowest surface temperature plot at 47.9 °C. Additionally, the upper and lower edges of the box represent the upper and lower quartiles of LST for each historical district, respectively, while the length of the box indicates the dispersion of LST within the districts. A longer box indicates a more dispersed distribution of LST within the historical district, reflecting greater variability. From Fig. 4, it is evident that the HC district exhibits the most dispersed distribution of LST and the greatest variability. In contrast, XST-BT demonstrates the most concentrated distribution of LST and the least variability.

3.3 Internal Analysis - Heterogeneity of LST Distribution within Historic and Cultural Districts

In addition to conducting a comparative analysis of the LST across various historical districts to discern regional variations, it is imperative to further scrutinize the internal heterogeneity of surface temperature distribution within these districts.

Figure 5 presents the clustering characteristics of cold and hot spots for LST within the study area, utilizing the ArcMap software platform. The distributions of cold and hot spots within the historic districts reveal the following features: The primary areas of cold spots within the districts are concentrated around bodies of water (SCH, XYK, and NLGX), cultural relics and ancient buildings (GZJ-YHG, and FYS), and the peripheries of modern and contemporary architectures (ZZZLN, ZZZLB, and DJMX). Conversely, the hot spots are primarily concentrated in regions where traditional residential architecture is prevalent. Actual images of typical cold and hot spots are presented in Fig. 6.

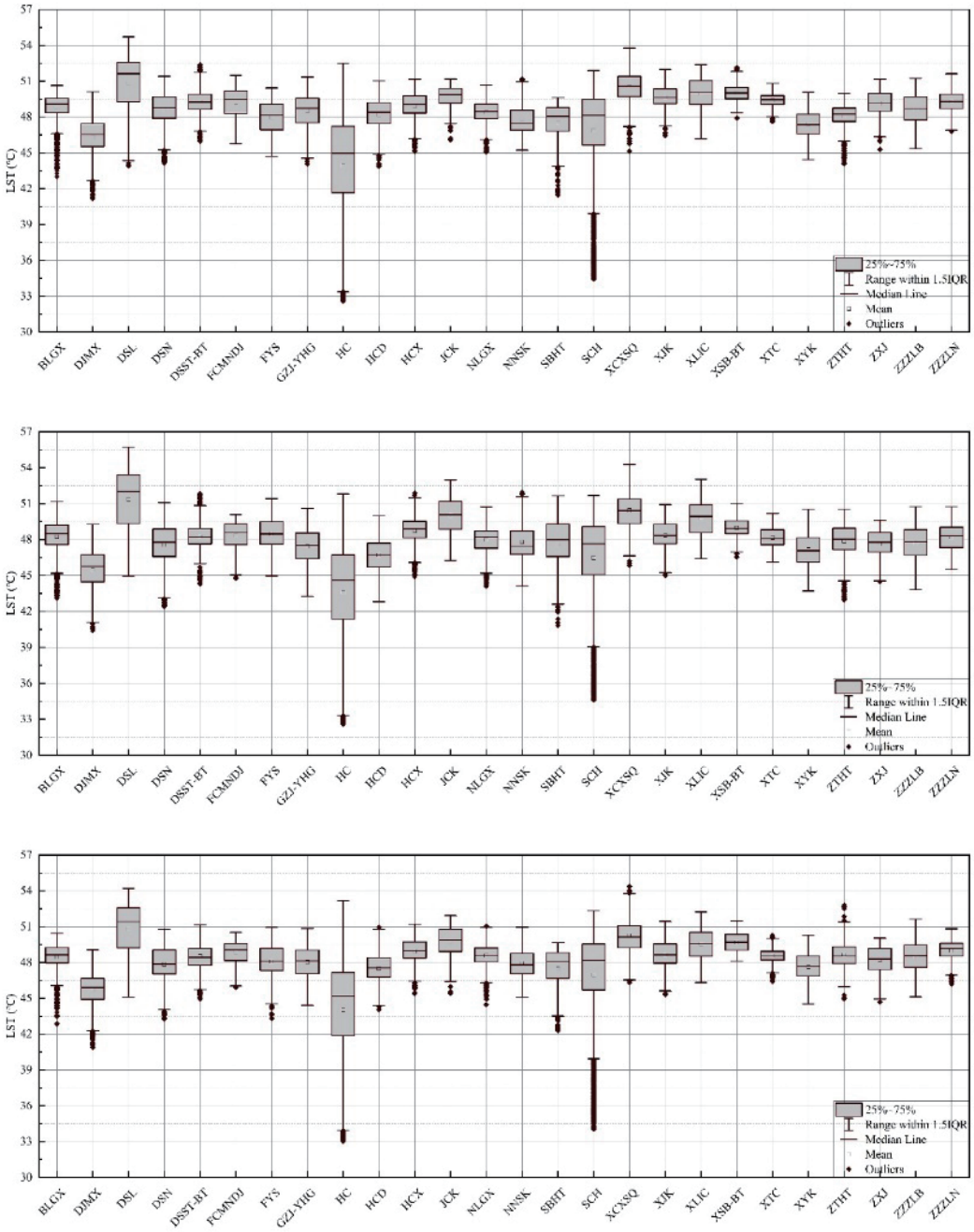

Fig. 4. (Color online) LST box plot analysis of historic districts in the years 2017, 2020, and 2023.

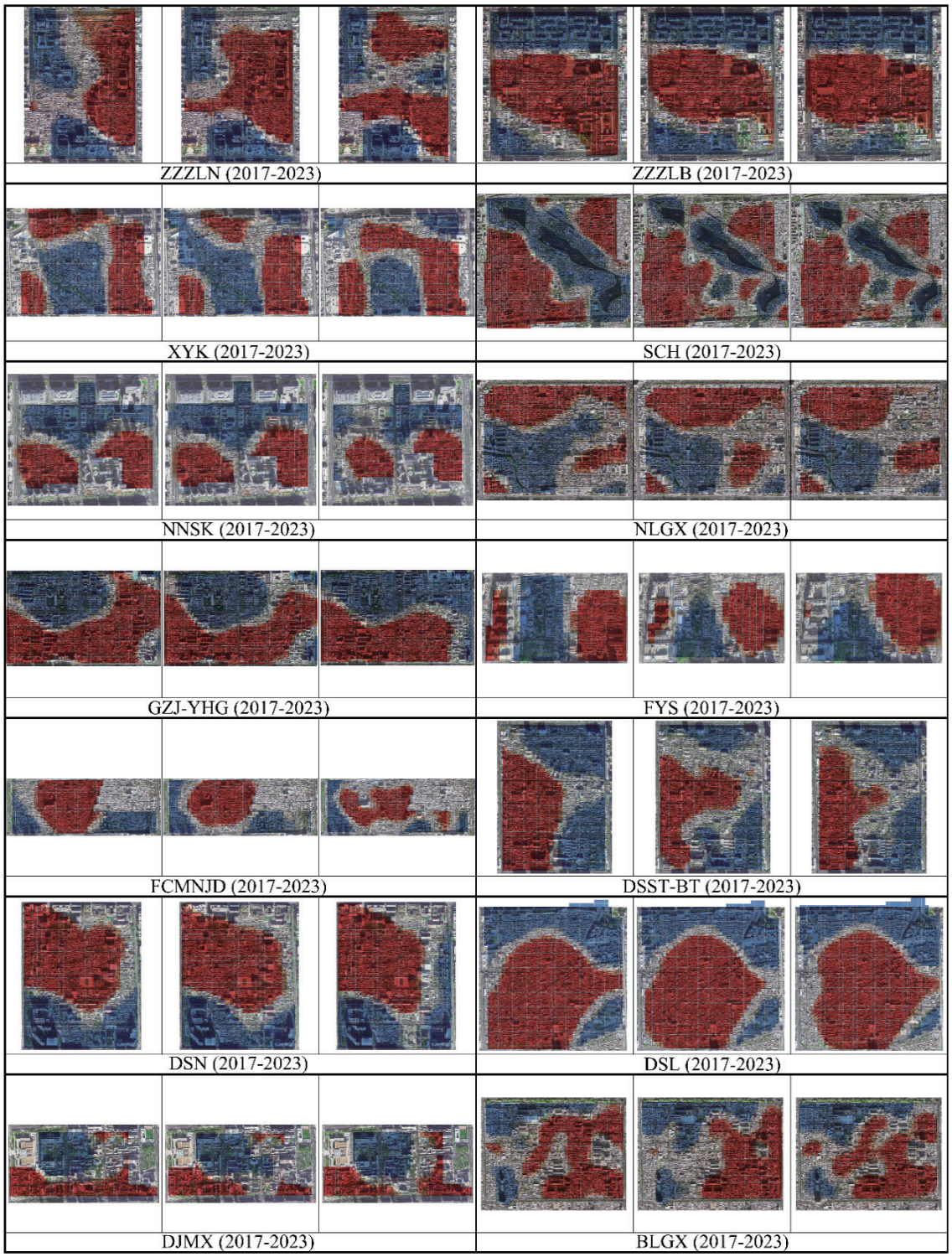

Fig. 5. (Color online) Analysis of the variation in LST within representative historic districts.

Fig. 6. (Color online) Cold and hot spots within the district.

4. Discussion

4.1 An exploration into the factors contributing to variations in land surface temperatures within historic districts

4.1.1 Urban form

The morphology of a street block is an assemblage of architectural, infrastructural, communal, and vegetative elements that are organized according to certain rules or principles, such as aspect ratio, street orientation, building density, height, plot ratio, and layout methods. Energy, embedded in the constructive codes of the block's morphology, signifies the formation of microenvironments dominated by the block's configuration.[22,23] In terms of the outcomes, this mode of action primarily includes two dimensions: promotion and suppression. Some research indicates that an increase in the aspect ratio facilitates heat dissipation and reduces the daily maximum temperature.[24] Meanwhile, the results of research based on the heat island effect of semi-enclosed, dispersed, and strip-shaped spatial layouts show that although the high-rise point-like layout has a relatively high plot ratio, it is conducive to heat dissipation owing to its good shading effect and large open space, which can promote the flow of energy.[25,26] Meanwhile, some research studies also suggest that excessive building density can impede the city's spatial heat dissipation capacity.[23,24] Furthermore, land cover significantly affects the absorption and reflection of solar energy. For instance, vegetative cover absorbs solar radiation to drive photosynthesis, converting it into plant biomass and surface energy, while water bodies absorb more energy and affect the conductivity of the land surface thermal conductivity.[23,27]

Within the historical districts, the higher building density and lower architectural heights typical of traditional cultural neighborhoods contribute to a slightly elevated surface temperature compared with areas with lower densities and higher structures. This phenomenon also accounts for the cooler spots within the historical districts, which are primarily found around bodies of

water and modern architectural surroundings. Our further examination using linear regression analysis confirms the effects of building density, architectural height, and vegetation coverage on the historical and cultural districts. Notably, building density exhibits a significant positive correlation with the local LST in these districts, while architectural height, FVC, and LST show a notable negative correlation, aligning with previous research findings (Fig. 7).

4.1.2 Urban function

Different urban functional zones vary in energy consumption, spatial configurations, and population densities, which may consequently exert distinct effects on LST. In accordance with relevant planning documents and points of interest, we have delineated three distinct types of historical and cultural districts: scenic, commercial, and residential (Table 2). A boxplot analysis of these three functional categories reveals that scenic districts exhibit the lowest average LST and the greatest dispersion in LST values, commercial districts display the highest average LST, and residential districts show the least dispersion in LST (Fig. 8).

4.2 Environmental value of historic architectural structures

From Fig. 6, it is evident that cold spots in historical districts are primarily located in the vicinity of cultural relics and ancient buildings, indicating that the forefathers considered climate adaptability in the construction of traditional architecture. Allow me to elaborate.

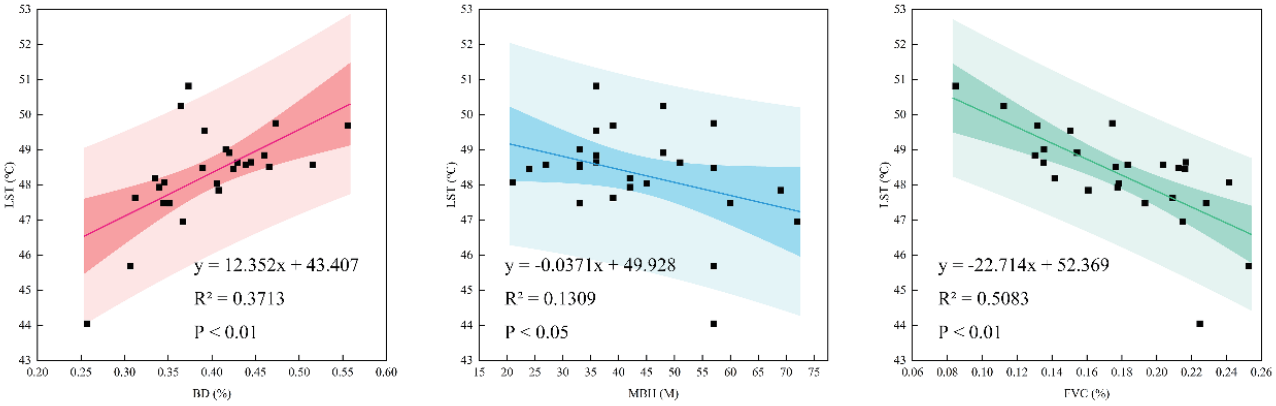

Fig. 7. (Color online) Linear regression equation of urban morphological parameters and LST.

Table 2
Classification of functional types in historic cultural districts.

District type	Historical cultural district
Scenic spot	HC, FYS, SCH, GZJ-YHG, DJMX
Commercial	DSL, XYK, XLIC, NLGX, XCXSQ
Residential	XSB-BT, DSST-BT, XTC ZZZLB, ZZZLN

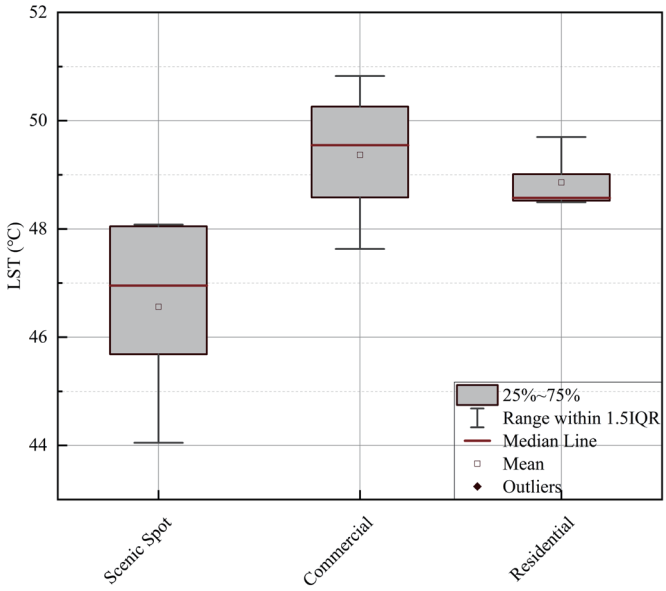

Fig. 8. (Color online) LST boxplot of historic districts with various functional types.

(1) Emphasis is placed on courtyard landscaping and flooring. In the greening of the courtyards of traditional Beijing Siheyuan, deciduous trees are predominantly chosen for their landscape (Fig. 9). These species, with their dense foliage in summer, serve to shield the interior from direct, scorching sunlight, providing shade and sun protection for the courtyard while offering a cool respite indoors. In winter, the trees lose their leaves, reducing obstruction of sunlight, allowing ample illumination for both the interior and the courtyard. The vegetation within the courtyard brings a host of benefits to the local climate and environment. Regarding flooring materials, bluish-gray bricks are commonly used, with a preference for a coarse finish (Fig. 9). These bricks, laid directly without polishing or trimming, feature wider joints that enhance their water absorption and retention capacity. Thus, watering the surface facilitates passive cooling.

(2) Emphasis is placed on the creation of transition spaces. In traditional Beijing Siheyuan, various elements such as verandas, screen partitions, sinking courtyards, and the like are employed to craft diverse forms of transition spaces (Fig. 10). These transition spaces not only enable the construction of intricate depth relationships, enhancing spatial interest, but also serve the function of shading, contributing to the creation of a conducive microenvironment.

(3) Architectural forms that incorporate climate adaptability are utilized. Initially, the walls of traditional Beijing Siheyuan are generally quite thick, constructed from a combination of earth, brick, and stone, with thicknesses reaching up to 490 mm. The thermal storage capacity and insulation performance of the adobe walls are particularly notable, enabling them to adapt well to the frigid winter conditions prevalent in Beijing.

The selection of window dimensions and forms in Beijing Siheyuan residences ensures that the northern side of the main room remains windowless, while large windows are positioned on

Fig. 9. (Color online) Typical landscape of courtyards in traditional Siheyuan. (Source: https://www.meipian.cn/j2w9kq8[28])

Fig. 10. (Color online) Verandas in Siheyuan. (Source: https://mt.sohu.com/20180511/n537383667.shtml[29])

the southern side for solar exposure. This design maximizes the building's exposure to sunlight during winter, facilitating optimal natural lighting. Additionally, it enhances the solar gain in the rooms, thereby increasing indoor comfort levels through thermal storage during the day, which in turn elevates the nighttime indoor temperature and reduces the heating load in winter.

The grand roofline of Beijing's Siheyuan is characterized by its "人" shape (Fig. 11), a design that offers several advantages. On one hand, the parabolic curve of this roofline facilitates rapid drainage. On the other, the sloping roof provides an effective buffer. In winter, cold outdoor air is channeled into the courtyard through the roof, undergoing a transition that shields the interior from direct chilling effects. Conversely, in summer, the sloping roof design prevents a sudden spike in indoor temperature caused by direct solar exposure, thereby ensuring a consistently comfortable thermal environment indoors.

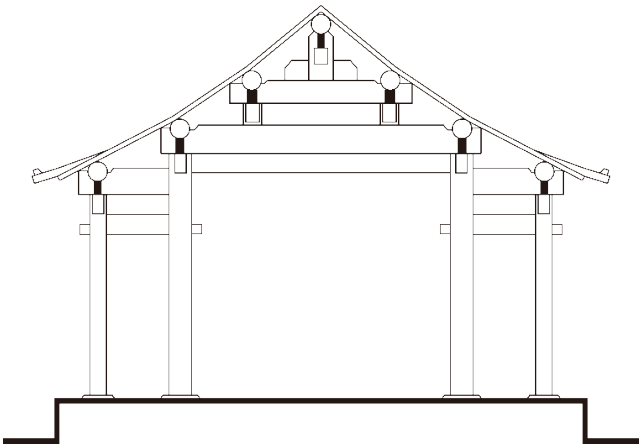

Fig. 11. Roof structure of Siheyuan buildings.

4.3 Planning and designing strategies for response

(1) Shading infrastructure

Effective shading infrastructure can significantly enhance the comfort of individuals within a space. In historical districts, we can leverage the preexisting trees, verandah, and cantilever to redesign and establish various shaded spaces of diverse scales and purposes (Fig. 12).

(2) The surface is to be paved with bricks and stones

The underlying surfaces surrounding a building directly affect the microclimate within the courtyard, with the choice of flooring and vegetation significantly impacting the building's energy consumption by affecting its microclimate. Within the historic districts, a brick and stone pavement stands out as a prominent feature in every corner. Moreover, bricks and stones possess the capability to absorb and retain heat, and the intervening gaps between them exhibit excellent permeability. Hence, the use of brick and stone pavements should be maximized (Fig. 13).

(3) Greening supplement

Greening is pivotal in ameliorating microclimates; however, the exceedingly high density of buildings in historical districts makes it challenging to establish extensive green spaces. Consequently, it is imperative to enhance pocket green spaces and vertical and rooftop greening to mitigate these challenges and mitigate the impact on the microclimate. Additionally, in historic districts, numerous residents engage in self-initiated greening efforts, and designers must not overlook the significance of these self-organized greening activities (Fig. 14).

(4) Demolition of illegal buildings

Currently, numerous unauthorized constructions exist within Beijing's historic and cultural districts, posing adverse impacts on the thermal environment of these areas. On one hand, these unauthorized constructions often exacerbate the already congested conditions of the narrow alleys, leading to increased densities of pathways and buildings, consequently raising

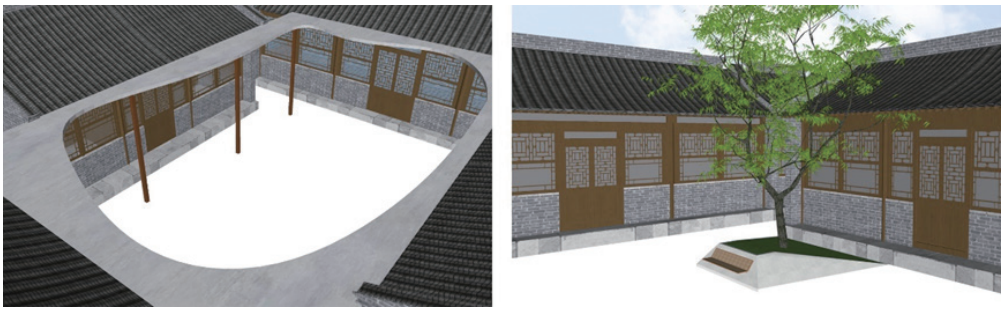

Fig. 12. (Color online) Shading infrastructure design strategies.

Fig. 13. (Color online) Pave design strategies.

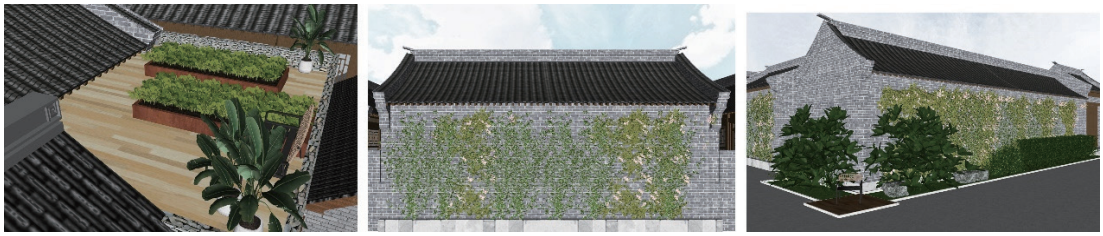

Fig. 14. (Color online) Greening design strategies.

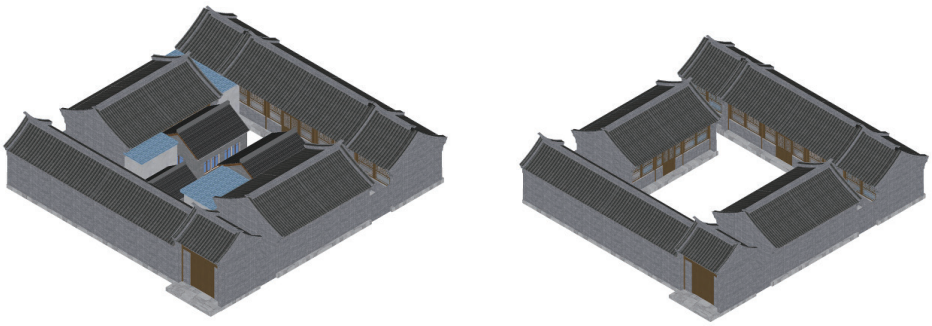

Fig. 15. (Color online) Demolition of illegal buildings.

energy consumption. On the other hand, these constructions frequently obstruct natural lighting and ventilation within the districts, impeding air circulation and making it challenging to dissipate heat. Therefore, it is imperative to systematically demolish these unauthorized buildings (Fig. 15).

5. Conclusion

In this research, we used the radiative transfer equation to study the surface temperature of 33 historic and cultural districts and seven proposed historic and cultural districts in the core area of Beijing, clarifying the differences in surface temperature between different historic districts and within historic districts. On the basis of the aforementioned research, we arrived at the following conclusions.

(1) In comparison with other areas within the core zone, the cultural and historical districts exhibit higher surface temperatures.
(2) In the study of all the historical and cultural districts discussed in this article, DSL exhibits the highest average surface temperatures in spatial terms, while the HC region registers the lowest. Temporally, the majority of the historical districts have experienced a decline in surface temperatures over the past six years. Notably, the most significant reduction in average LST has been observed in the areas from XJK, DSN, and DSST-BT over this six-year period.
(3) Within the historic districts, the hot spots of LST are predominantly located in the residential areas characterized by one-story buildings, while the cold spots are primarily concentrated around bodies of water, cultural relics, ancient architectural sites, and the peripheries of modern and contemporary buildings.

Acknowledgments

This study is funded by the Open Fund of Key Laboratory of Urban Spatial Information, Ministry of Natural Resources (Grant No. 2023PT002).

References

1 Y. Zhang and Y. Han: Heritage Sci. **10** (2022) 137. https://doi.org/10.1186/s40494-022-00776-5.
2 J. Zacharias, Z. Sun, L. Chuang, and F. Lee: Habitat Int. **49** (2015) 260. https://doi.org/10.1016/j.habitatint.2015.05.035.
3 Y. Wang, A. Agkathidis, and A. Crompton: Front. Archit. Res. **9** (2020) 751. https://doi.org/10.1016/j.foar.2020.07.003.
4 C. Zhang and B. Lu: Travel Behav. Soc. **5** (2016) 23. https://doi.org/10.1016/j.tbs.2015.08.001.
5 G. Pavlendová, J. Šujanová, D. Cagáňová, and R. Nováková: Mobile Networks Appl. **25** (2020) 876. https://doi.org/10.1007/s11036-020-01521-7.
6 N. Li, Z. Guo, W. Geng, L. Li, and Z. Li: Sustainable Cities Soc. **99** (2023) 104927. https://doi.org/10.1016/j.scs.2023.104927.
7 M. Li and C. Feng: Heliyon **9** (2023) e19552. https://doi.org/10.1016/j.heliyon.2023.e19552.
8 S. Wang, J. Zhang, F. Wang, and Y. Dong: Sustainable Cities Soc. **98** (2023) 104790. https://doi.org/10.1016/j.scs.2023.104790.
9 W. Su, L. Zhang, and Q. Chang: Build. Environ. **225** (2022) 109600. https://doi.org/10.1016/j.buildenv.2022.109600.
10 J. Liu and A. Deguchi: Front. Archit. Res. **14** (2024) 928. https://doi.org/10.1016/j.foar.2024.03.008.
11 J. Cristóbal, J. C. Jiménez-Muñoz, J. A. Sobrino, M. Ninyerola, and X. Pons: J. Geophys. Res. **114** (2009). https://doi.org/10.1029/2008JD010616.
12 J. C. Jimenez-Munoz, J. Cristobal, J. A. Sobrino, G. Soria, M. Ninyerola, and X. Pons: IEEE Trans. Geosci. Remote Sens. **47** (2009) 339. https://doi.org/10.1109/TGRS.2008.2007125.
13 N. Sahani, S. K. Goswami, and A. Saha: Spatial Inf. Res. **29** (2021) 519. https://doi.org/10.1007/s41324-020-00372-4.
14 A. Zarei, R. Shah-Hosseini, S. Ranjbar, and M. Hasanlou: Adv. Space Res. **67** (2021) 3979. https://doi.org/10.1016/j.asr.2021.02.019.
15 A. S. Athick, K. Shankar, and H. R. Naqvi: Data Brief. **27** (2019) 104773: https://doi.org/10.1016/j.dib.2019.104773.
16 N. Chang, K. Bai, S. Imen, C. Chen, and W. Gao: IEEE Syst. J. **12** (2018) 1341. https://doi.org/10.1109/JSYST.2016.2565900.
17 F. Mumtaz, Y. Tao, G. Leeuw, L. Zhao, C. Fan, A. Elnashar, B. Bashir, G. Wang, L. Li, S. Naeem, A. Arshad, and D. Wang: Remote Sens. **12** (2020) 2987. https://doi.org/10.3390/rs12182987
18 Y. Zhao, D. Ponzini, and R. Zhang: Habitat Int. **96** (2020) 102106. https://doi.org/10.1016/j.habitatint.2019.102106.
19 T. Vural-Arslan and A. Cahantimur: Futures **43** (2011) 361. https://doi.org/10.1016/j.futures.2011.01.003.
20 N. Li, F. Zhang, W. Geng, and Z. Li: J. Build. Eng. **72** (2023) 106342. https://doi.org/10.1016/j.jobe.2023.106342.
21 A. Getis and J. K. Ord: Geogr. Anal. **24** (1992) 189. https://doi.org/10.1111/j.1538-4632.1992.tb00261.x.
22 T. McPhearson, D. Haase, N. Kabisch, and Å. Gren: Ecol. Indic. **70** (2016) 566. https://doi.org/10.1016/j.ecolind.2016.03.054.
23 R. Lemoine-Rodríguez, L. Inostroza, and H. Zepp: Sci. Total Environ. **830** (2022) 154570. https://doi.org/10.1016/j.scitotenv.2022.154570.
24 Z. Zhang, W. Luan, J. Yang, A. Guo, M. Su, and C. Tian: Urban Clim. **49** (2023) 101553. https://doi.org/10.1016/j.uclim.2023.101553.
25 H. Zhang, C. Wang, H. Yang, and Z. Ma: Ecol. Indic. **161** (2024) 111972. https://doi.org/10.1016/j.ecolind.2024.111972.
26 Y. Mo, Y. Bao, Z. Wang, W. Wei, and X. Chen: Build. Environ. **257** (2024) 111545. https://doi.org/10.1016/j.buildenv.2024.111545.
27 Q. Yang, X. Huang, J. Yang, and Y. Liu: Environ. Res. Lett. **16** (2021) 024032. https://doi.org/10.1088/1748-9326/abdaed.
28 Meipian: https://www.meipian.cn/j2w9kq8 (accessed December 2017).
29 Sohu: https://mt.sohu.com/20180511/n537383667.shtml (accessed May 2018).